Earth, Planets and Space

FULL PAPER

Open Access

Statistical and simulation study on the separation in junction frequencies between ordinary (O) and extraordinary (X) wave in oblique ionograms

Sun FengJuan[1,2], Wan XianRong[1*], Zhang HongBo[2], Zhou Bao[2], Ban PanPan[2,3] and Cao Hongyan[2]

Abstract

The most important aim in interpreting an oblique ionogram is to obtain the accurate Junction Frequencies (JFs) of the ordinary (O) and extraordinary (X) mode. This requires the correct identification of O- and X-mode traces, so it is very helpful and worthy to grasp the relative position between the two modes. This paper presents a statistical and simulation study of the separation in JFs between O- and X-waves based on observed oblique ionograms over three mid-latitude paths within China and a 3D ray-tracing program. The dependence on local time, season, geomagnetic activity, O-wave JF and group path, solar activity, direction, and length of propagation is investigated. The main conclusions are as follows: (a) the separation on east–west path is susceptible to ionospheric variability, while the separation on north–south path does not show a significant correlation with local time and season; (b) a general diurnal tendency and a summer anomaly on east–west propagation are first proposed and discussed, which may be related to the diurnal variation of hmF2 above the reflection point and the strong lower layers below the reflection point; (c) the separation varies approximately as a cosine function with the propagation direction owning two maxima in the north–south direction and two minima in the east–west direction; (d) the variation patterns of the separation with the propagation length are obviously not the same in different directions. In the case of east–west propagation, the separation decreases to a minimum near ground range of 2000 km and then increases very slowly with increasing ground range, while it monotonically increases for the north–south propagation path.

Keywords: Ionosphere, Oblique sounding, Oblique ionogram, Junction frequency, Ordinary wave, Extraordinary wave

*Correspondence: xrwan@whu.edu.cn

[1] Radio Detection Research Center, School of Electronic and Information, Wuhan University, Wuhan 430072, China
Full list of author information is available at the end of the article

Graphical Abstract

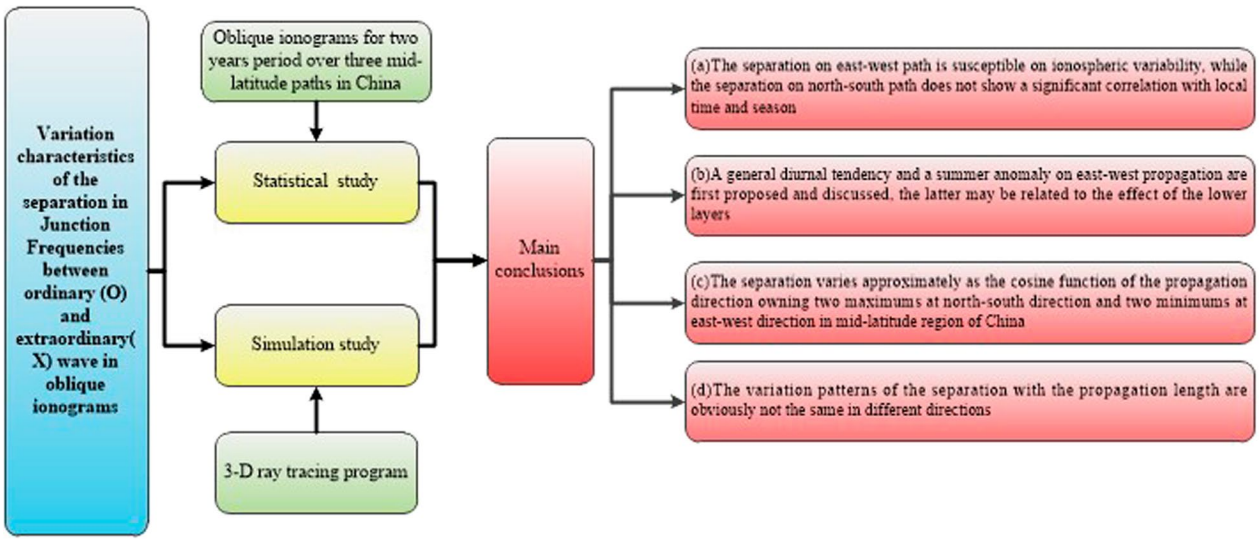

Introduction

Oblique incidence ionospheric sounding (Davies 1990), which consists of a transmitter and a receiver located several hundreds or thousands of kilometers apart, is a powerful tool for monitoring the prevailing propagation conditions in real time and is also important for tracking ionospheric effects caused by space weather events. It offers several important advantages over vertical sounding, such as the opportunity of monitoring the ionosphere across large, otherwise inaccessible areas such as ocean surfaces, and the ability of a receiver to detect signals from many different directions (Ippolito et al. 2015a, b). So it is widely used for propagation predictions of high frequency (HF) radio communications, over-the-horizon radar localization and for basic research purposes (Rao 1973; Yau et al. 2006; Chemogor et al. 2020; Rogov et al. 2021). Heitmann et al. (2018) regarded oblique sounding as the most efficient tool for determining the characteristics of HF channel.

The oblique ionogram, a group path or time delay versus operating frequency record, contains useful information regarding the state of the ionosphere over the range of the signals traverse (Reily and Kolesar 1989; Phanivong et al. 1995; Ippolito et al. 2015a, b). The important characteristics like the LOF (the Lowest observed frequency), MOF (the Maximum observed frequency), FMUF (the highest useable frequency of one-hop F layer), FHLOF (the lowest observed frequency of the high-angle ray along one-hop F layer), FLLOF (the lowest observed frequency of the low-angle ray along one-hop F layer), and 2FMOF (the maximum observed frequency of the two-hop F layer) can be scaled from an oblique ionogram. Among these, the FMUF, known as the basic MUF or Junction Frequency (JF) of one-hop F2 trace, is the most important one, who decides the highest frequency at which a radio wave can propagate between given terminals by ionospheric propagation alone (Pezzopane and Pietrella 2008). In an oblique ionogram, the JF corresponds with the frequency at which the high- and low-angle rays join.

Due to the Earth's magnetic field, the ionosphere is a doubly refracting medium. It can be observed that two distinct ionospheric echo traces exist in an oblique ionogram, which are so-called ordinary(O) and extraordinary (X) wave traces. The JFs of the O- and X-waves are obviously different as shown in Fig. 1. Although it is sufficient to extract only the O-wave JFs for most applications, there are still some occasions that the O- and X-wave parameters need to be accurately extracted simultaneously, such as studying the ionospheric response to the geomagnetic field, improving the inversion accuracy of electron density in the lower ionosphere (Storey 1960), etc. However, the processing and interpretation of OIS (oblique-incidence sounder) ionograms is more complicated than that of VIS (vertical-incidence sounder) ionograms. Using a polarimetric receive antenna, the O- and X-modes can be well separated on a VIS, but the separation of these two modes for an OIS is more difficult owing to the variable separation in phase difference between the two modes (Harris et al. 2017). In addition, due to the influences of the random time-varying nature of the ionosphere and harsh electromagnetic environment, the F-layer O- or X-wave trace is usually submerged by noise

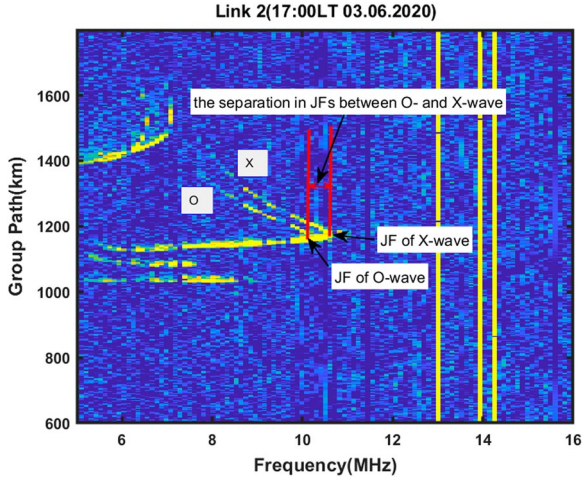

Fig. 1 An oblique ionogram indicating JF, O- and X-wave traces, the separation in JFs between O- and X-wave

or interference in oblique ionograms. Then, it is difficult to obtain sufficient scalable ionograms to provide a physically relevant measurement of the O- and X-wave JFs. In this case, it is useful to master the specific characteristics of the separation in JFs between O- and X-wave, which can be helpful in automatically identifying O- and X-wave parameters.

As early as 1970, Bradley et al. (1970) pointed out that the JF separation between O- and X-wave merited further investigation, and it should be established how it varied with path, latitude, mode order, and direction of propagation. Since then, many scholars have carried out in-depth research. Agy and Davies (1959) found that this separation decreased with an increase in distance for the case of east–west path, which gradually changed from 0.7 MHz of the vertical sounding scene to about 0.2 MHz on a 2400 km path. Magneto-ionic splitting of O- and X-components was also studied by Kopka and Moller (1968) using ray tracing and a flat Chapman layer. Results were given for a 2000 km path as a function of both magnetic latitude and magnetic azimuth, showing that: (1) the magneto-ionic splitting was less for an east–west path than a north–south path; (2) for a transmission in the direction of the magnetic meridian (north–south path), the magneto-ionic splitting decreased with increasing magnetic latitude; (3) for a transmission transverse to the meridian, the splitting was zero at the equator and increased towards the pole. Davies (1990) presented the relationship between the JFs of the O- and X-wave (referred as f_O and f_X, respectively) reflected for the cases of trans-equatorial and magnetic east–west propagation, which were $f_X - f_O \approx f_H cosI$ and $f_X - f_O \approx f_H^2/2f_O$ (I is the magnetic dip, f_H is the electron gyrofrequency), respectively. An explicit formula about the separation in JFs between O- and X- wave (abbreviated as $f_X - f_O$) as a function of local magnetic dip and propagation azimuth was obtained by Bennett and Dyson (1994) for long paths, and they also showed how to use analytic ray tracing to determine the separation for shorter paths. Lundborg et al. (1995) found that the separation varied with propagation distance and maximum observed frequency (MOF), changing between 0.7 MHz when MOF was low (about 5 MHz) and 0.4 MHz when MOF was high (about 15 MHz) for propagation over the path Kiruna to Uppsala.

So far, most scholars have analyzed the variability of the separation in JFs between O- and X-wave from different aspects, and there is still a lack of systematic and comprehensive analysis. As a continuation of the study, the present paper focuses on the variation characteristics of the separation with local time, season, geomagnetic activity, O-wave JF and group path, solar activity, direction, and length of propagation. The contributions of this article lie as follows:

(1) The dependence of the separation on local time, season, geomagnetic activity, O-wave JF, and group path are statistically analyzed based on observed oblique ionograms over three mid-latitude paths within China. A general diurnal tendency and a summer anomaly on east–west propagation are first proposed and discussed.
(2) The influences of the length of the propagation circuit, the direction of propagation, and the solar activity variability have been analyzed by a ray-tracing program. A different variation pattern of the separation with the propagation length is presented which is partly inconsistent with previous results.

This article is organized as follows. The source of the data and the plan of the experiment are briefly described in "Data sets". Then, the method of analysis and statistical results obtained for two years over three mid-latitude paths within China are presented in "Data analysis and results". In "Discussions", we discuss the presented results and investigate the effects of solar activity, direction, and length of propagation on the separation by 3D ray-tracing. Finally, the conclusion is drawn in "Summary and conclusions".

Data sets

The data sets were collected by an oblique sweep-frequency pulse transmission experiment carried out by the China Research Institute of Radio-wave Propagation

(CRIRP). In this experiment, three transmitters and one receiver were deployed in the middle of China to establish three radio paths, as shown in Fig. 2. The three paths were arranged with different orientations and basically the same length, about 1000 km. The receiver system was located at Xi'an and three transmitters were located at Lianyungang, Deqing, and Linchuan separately. The configuration was beneficial in observing the influence of the propagation direction on O- and X-wave JFs. Table 1 gives the location, azimuth, and length of each path. The geomagnetic azimuths of the paths range from 90.1° to 141.6°, and correspondingly the propagation turns east–west propagation to quasi south-north propagation.

The instruments used for this experiment were designed and manufactured by CRIRP. They were essentially the same as that used for sweep-frequency echo sounding of vertical incidence covering the frequency range from 3 to 30 MHz with a sweep rate of 50 kHz s^{-1}. The main difference was that the antennas used to transmit and receive signals were horizontally polarized log-periodic antenna and horizontal dipole antenna in this case, while delta antenna and orthogonal inverted V antenna were used for vertical sounding. Furthermore, the high-precision Global Positioning System (GPS) was employed to provide the system timing ensuring that the transmitter and receiver were synchronized with an accuracy better than 10 μs and also allowing absolute time of flight measurements to be made.

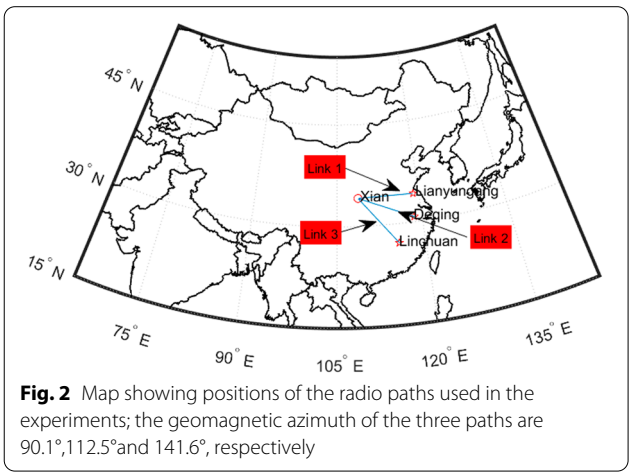

Fig. 2 Map showing positions of the radio paths used in the experiments; the geomagnetic azimuth of the three paths are 90.1°,112.5°and 141.6°, respectively

The experimental system used a low-power, pulse compression waveform and made extensive use of digital signal processing techniques in order to measure channel parameters and obtain the oblique ionograms. The maximum output power of the transmitter was 400 W. A maximal length pseudo-noise sequence (M-sequence) of length 255 or 511 chips modulated onto a bi-phase PSK carrier was employed to offer a processing gain of about 24 dB or 27 dB. The duration of each chip was 25 μs giving a signal bandwidth of 40 kHz and a corresponding range resolution of 7.5 km. The entire M-sequence lasted for 6.375 ms or 12.775 ms. The repetition period of the pulse was 25 ms. In order to improve the signal-to-noise ratio, the coded pulses were sent 5 times at each frequency.

Since IRI did not model foF2 (ionospheric F-region critical frequency) correctly during 2008–2009 than during 2010–2016 (Luhr and Xiong 2019), we mainly focused on the variation of FMUF in low solar activity. The experiment was organized and carried out during two periods, 2008 interval and 2020 interval, with an annual averaged sunspot number of 4.2 and 8.8, respectively. The first period ran from January to December 2008, and the measurements were performed round the clock during local time 8:00–19:00 every day with a 15 min interval. That means that the system operates only in daytime and generates one oblique ionogram for each path every 15 min. On the second period, measurements were performed once a quarter-hour for 24 h a day during 2020. The JFs of the O- and X-wave were manually extracted for every oblique ionogram on each path, in which the O- and X-mode traces can be successfully identified. In order to ensure the accuracy of the JFs, We excluded ionograms that the O- and X-mode traces incomplete or diffused, such as ionograms with spread F. A total of 119,604 oblique ionograms were collected during the experiment, and 78,783 groups of JF were successfully extracted, accounting for about 65.9% of total ionograms. Among the discarded ionograms, there were 19,974 ionograms with spread F, which was about 16.7% of total ionograms. In addition, the peak height of the F2-layer (represented by hmF2) and the 3-hourly Kp

Table 1 Detail of the radio links used in the investigation

Radio path	Transmitter	Receiver	Geographic Azimuth (degree)	Geomagnetic Azimuth (degree)	Path length (km)
Link 1	Lianyungang	Xi'an	86.8°	90.1°	946
Link 2	Deqing	Xi'an	109.3°	112.5°	994
Link 3	Linchuan	Xi'an	138.4°	141.6°	1004

index in the corresponding time period were obtained to analyze the relationships between the separation $f_X - f_O$ with diurnal variation of the ionosphere and the geomagnetic activity. The hmF2 is estimated from the ionograms obtained by TYC-2 ionosonde located in Xi'an. The TYC-2 ionosonde manufactured by the CRIRP is a digital ionosonde similar to the widely used Digisonde Portable Sounder 4 (DPS-4) ionosonde, which is an upgraded version of TYC-1 ionosonde (Wang et al. 2018). The 3-hourly Kp index was provided in the Web site: http://wdc.kugi.kyoto-u.ac.jp/.

Data analysis and results

Direction variability

The probability density of the separations in JFs between O- and X-wave is firstly investigated to obtain an overall picture of Magneto-ionic splitting variation over three radio links, as shown in Fig. 3. For Link 1, a magnetic east–west propagation path, the separation $f_X - f_O$ changes between 0.1 MHz and 0.5 MHz, and mainly concentrates in 0.15–0.35 MHz. The separation for Link 2 (the southeast-northwest propagation path) varies from 0.2 MHz to 0.7 MHz with a mean value of 0.4 MHz and for Link 3(the quasi south–north propagation path) it varies between 0.3 MHz and 1.0 MHz with a mean value of 0.67 MHz. It is obvious that the $f_X - f_O$ increases as the propagation direction deviating from the direction of east–west. This statistical feature is consistent with previous research results that the magneto-ionic splitting is less for an east–west path than for a north–south path.

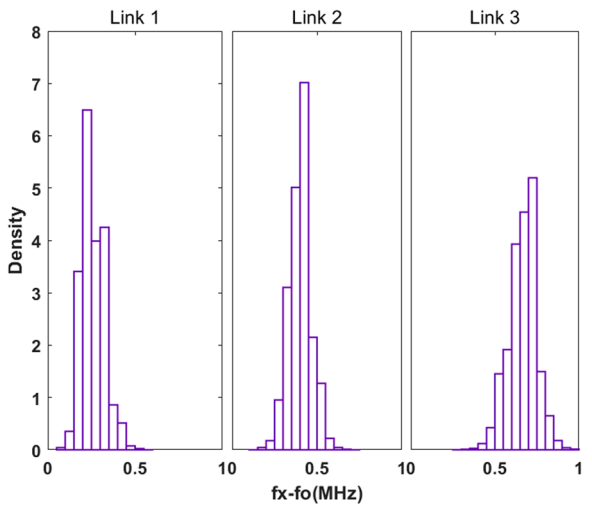

Fig. 3 Probability density of the separations observed through three radio links

Local-time variability

The JFs data observed in the two periods are grouped together and are binned as a function of local time (LT) with an interval of 1 h. The variation of the separation $f_X - f_O$ over three radio links against LT is presented separately in Fig. 4. It can be found that the diurnal tendencies of the separation on the three paths exhibit different patterns. Although the standard deviation is relatively large, the mean separation on Link 1 shows an obvious general diurnal variation. It increases after sunrise, has peak near local noon, decreases during the afternoon, and then increases again, reaching a high level at local midnight or early morning. The difference between the maximum and minimum mean separation is about 0.08 MHz on Link 1, which is nearly twice the average standard deviation. The mean separation on Link 2 shows a weak diurnal variation with a rise after sunset and the maximum variation is about 0.06 MHz, comparable with the standard deviation (the mean standard deviation is about 0.051 MHz). However, the separation on Link 3 presents no obvious day–night asymmetry and varies around the mean value throughout the whole day. It can be concluded that the magneto-ionic splitting on the east–west propagation link is more susceptible to LT variability compared with the north–south propagation. It is necessary to stress that the variation in hourly average on Link 3 is less than (or comparable with) the system frequency resolution, which is 0.05 MHz.

Seasonal variability

To evaluate the dependence of the separation $f_X - f_O$ on seasons, the JFs are sorted into the following four seasonal bins just as Wang et al. (2018): summer (May, June, July, and August), spring (March and April), autumn (September and October), and winter (January, February, November, and December). The hourly mean of the separations in each bin is calculated for each radio path. The statistical results are shown in Fig. 5. The following common features could be found: (1) the seasonal distribution pattern on Link 3 is obviously different from Link1 and 2; (2) the average separations on Link 1 and 2 during the daytime in summer are about 0.06 MHz and 0.04 MHz higher than other seasons respectively, while there is no significant seasonal difference on Link 3; (3) On Link 1, the average standard deviation of the separation in spring, summer, autumn, and winter is 0.046 MHz, 0.05 MHz, 0.046 MHz, and 0.045 MHz respectively, and the standard deviations of Link 2 and 3 are accordingly 0.05 MHz and 0.08 MHz,0.053 MHz, and 0.087 MHz, 0.051 MHz and 0.083 MHz, 0.05 MHz and 0.081 MHz; (4) For Link 1 and 2, the largest separation in the day occurs at night in most seasons except

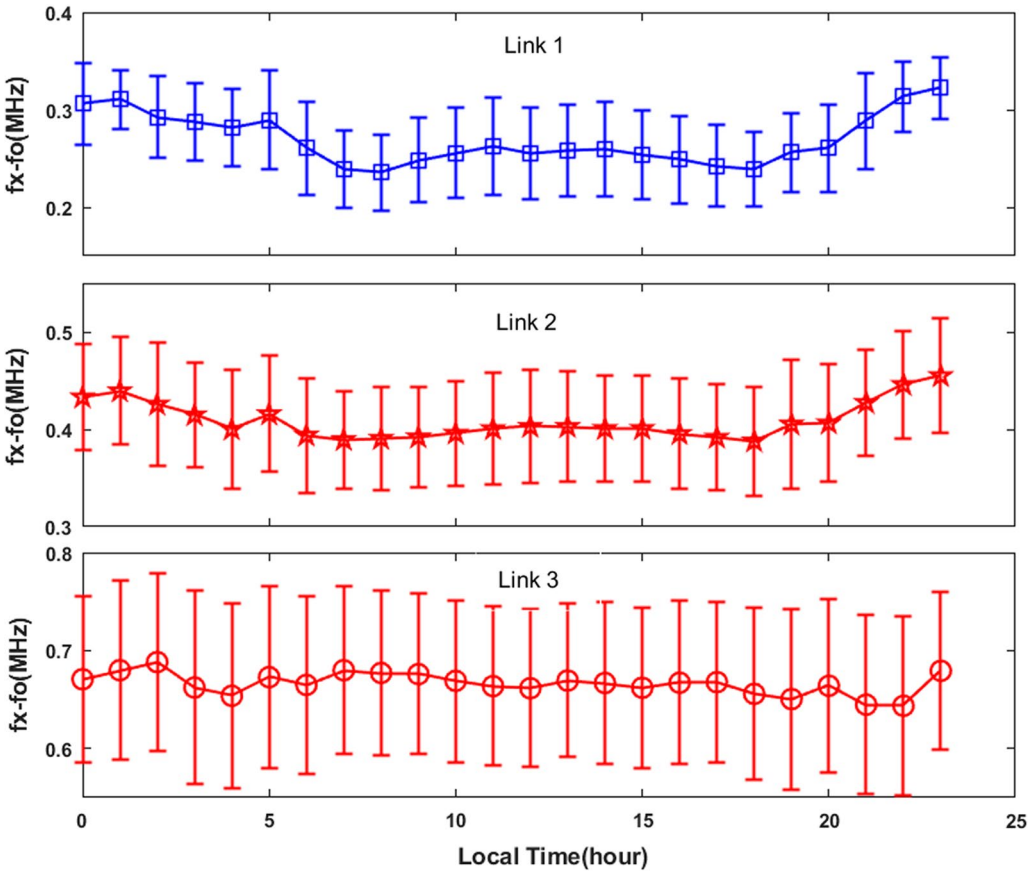

Fig. 4 Local time variation of the separations observed through three radio links

summer, when the most dominant separation are present during daytime(denoted as summer anomaly). This statistical feature suggests that the seasonal variability of the separation in case of the east–west propagation is more prominent than that on the north–south path.

Geomagnetic activity

Diurnal variation of a 3-hourly Kp index is employed for studying the dependence of the separation $f_X - f_O$ on geomagnetic variability. The data are categorized into two sets of quiet and disturbed conditions of geomagnetic activity. Based on Davies' relationships between the JFs of the O- and X-wave reflected for the cases of trans-equatorial and magnetic east–west propagation in "Introduction", it is known that the separation is mainly affected by the changes of the gyrofrequency f_H and the O-wave's JF f_O due to geomagnetic disturbance. Considering that general geomagnetic disturbance cannot cause a significant change in f_H and f_O, we refer to the display threshold of Kp index in the American space weather prediction center, and take Kp < 4 as a quiet condition. If the maximum value of the 3-hourly Kp index in a day is greater than 4, the day is considered as a disturbed day and the data observed during the day is classified into the disturbed set. Figure 6 shows the daily maximum Kp indices in 2008 and 2020. Observations from Fig. 6 show that there are only about ten percent of the times with geomagnetic disturbance during the two experimental periods. The mean value of the separations in each bin is calculated separately for each radio link shown in Fig. 7. The separation in geomagnetic disturbed condition is slightly smaller than that in the case of geomagnetic quiet condition by about 0.01 MHz (less than the system resolution) on Link 1 and 2. But there is no pronounced dependence on Link 3.

O-wave JF and group path variability

In order to analyze the correlation between the separation $f_X - f_O$ and the O-wave JF and group path, the JFs are binned as a function of O-wave JF from 3 to 22 MHz in steps of 3 MHz and as a function of O-wave group path from 1000 to 1450 km in steps of 50 km. The statistical mean of the separations is calculated as the ratio of the summation of the observed separations to the

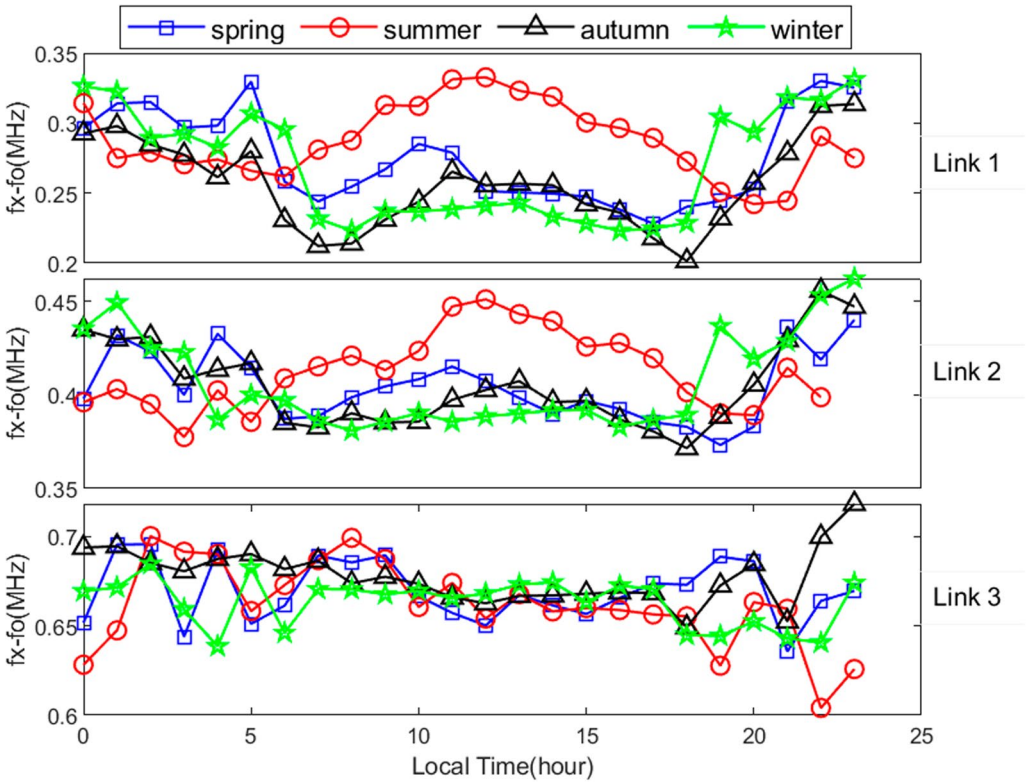

Fig. 5 Seasonal variation of the separations observed through three radio links; blue, red, black, and green lines represent spring, summer, autumn, and winter, respectively

total number of separations in each bin. Figures 8 and 9 show the variation of the separation compared with the O-wave JF and group path, respectively. Observations from Fig. 8 show that for all cases the separation initially decreases with increasing O-wave JF, but for the cases of Link 2 and 3, the separation decreases to a minimum and then increases very slowly with a total deviation less than the frequency resolution. Figure 9 shows that the separation increases with a decrease in the O-wave group path on Link 1 and 2, and slightly decreases on Link 3. It is evident that the separation in the case of east–west propagation is more susceptible to the O-wave JF and group path.

Discussions

In the above analysis, we have focused on the statistical characteristics of the separation in JFs between O- and X-wave in the mid-latitude China region. The statistical mean, local time, season, geomagnetic activity, O-wave JF, and group path dependence are analyzed. The presented results are, in general, consistent with the previous theoretical and experimental results (Agy and Davies 1959; Kopka and Moller 1968; Davies 1990; Bennett et al. 1994; Lundborg et al. 1995). However, some new findings in the above statistical investigation are worth further discussions.

Case of east–west propagation

The statistical investigations among the three paths show that the separation on the east–west path is minimal, but its relative change is much more prominent and more susceptible to local-time and seasonal variability. Figures 4 and 5 demonstrate that the separation on the east–west path regularly changes with local time. In general, the separation gradually increases after sunrise with one maximum near local noon, then slowly decreases before sunset, and grows up until reaching another maximum at midnight or pre-sunrise, and then decreases again with one minimum between 7:00 LT and 8:00 LT. According to the Appleton–Hartree formula with no collisions (Davies 1990), the refractive indices of the O- and X-modes are almost the same when a radio ray just enters the ionosphere. As the ray continues to pass through deep, the difference in the refractive index of the two modes becomes larger, and the propagation paths become more and more different. Therefore, we conjecture that the diurnal variation of the separation is related to the diurnal variation of hmF2 (the height of

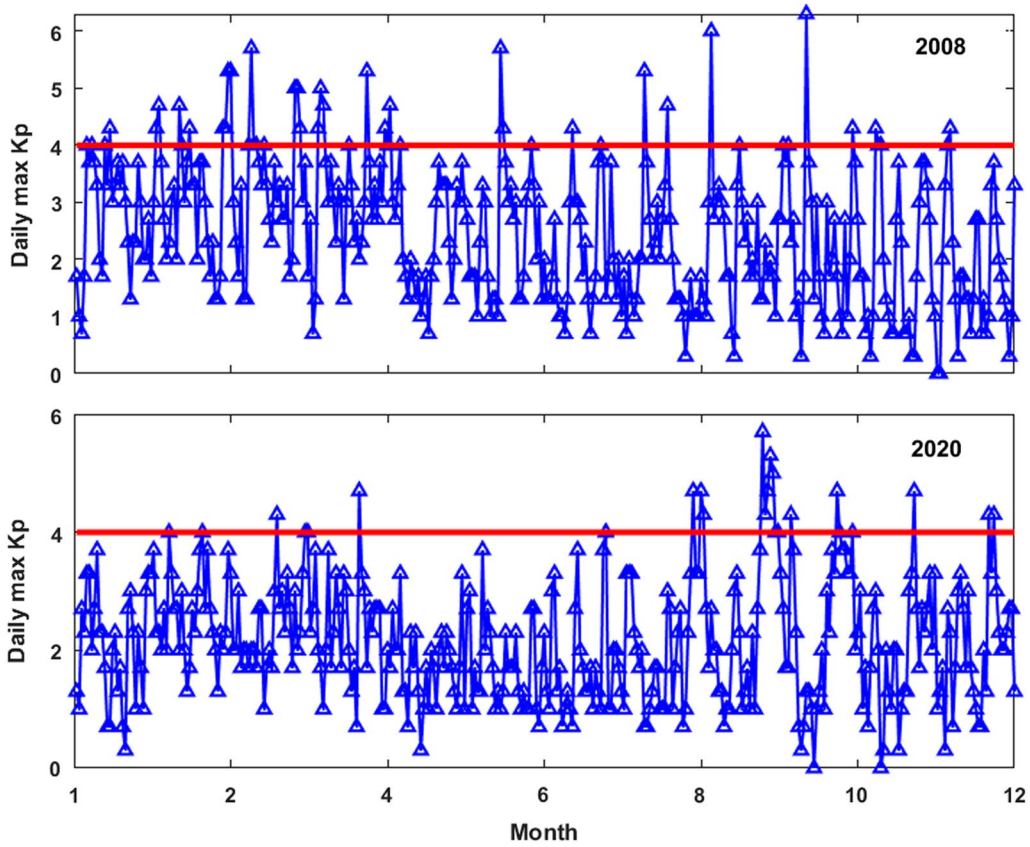

Fig. 6 Daily max Kp indices in 2008 and 2020, red solid line indicates Kp = 4

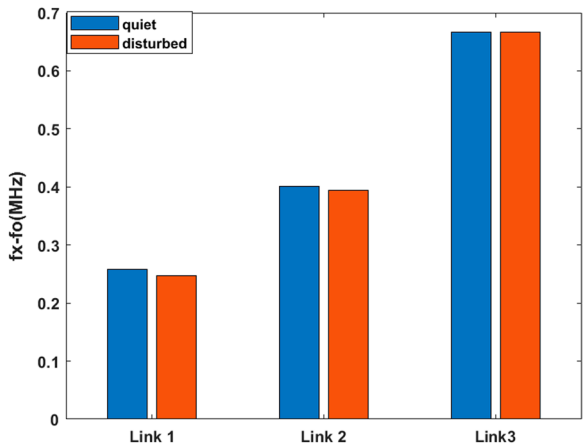

Fig. 7 Geomagnetic variability of the separations observed through three radio links

the peak electron density of F2-layer, see more details in Davies 1990). Then, we analyze the seasonal variation of hmF2 observed in Xi'an (one end of Link 1), as shown in Fig. 10. Comparing Fig. 10 with the top graph of Fig. 5, it can be found that the diurnal variation trend of the separation $f_X - f_O$ is highly similar to that of hmF2, especially in spring, autumn and winter. At night, when hmF2 goes higher, the separation becomes larger. After sunrise, when hmF2 decreases to a minimum, the separation is also minimized. At noon, when hmF2 rises to a maximum, the separation increases to a maximum too. This means that the separation varies quasi-linearly with hmF2. However, the linear relationship between separation and hmF2 in summer is no longer satisfied, in which case the hmF2 during daytime is comparable with that at night, while the separation at daytime is significantly larger than the nighttime separation.

The typical daytime oblique ionograms in spring and summer are reviewed to seek for possible explanations. Figure 11 presents a typical set of oblique-incidence F2-layer traces at 12:50 LT. The F2-layer trace circled by a red ellipse was taken on August 7, 2010 and the trace circled by a white ellipse was taken on March 7, 2010. Comparing these two sets of F2-layer traces, we find that the group path in summer is about 110 km higher than that in spring. It can be inferred that the difference between the equivalent reflection height of the F2-layer

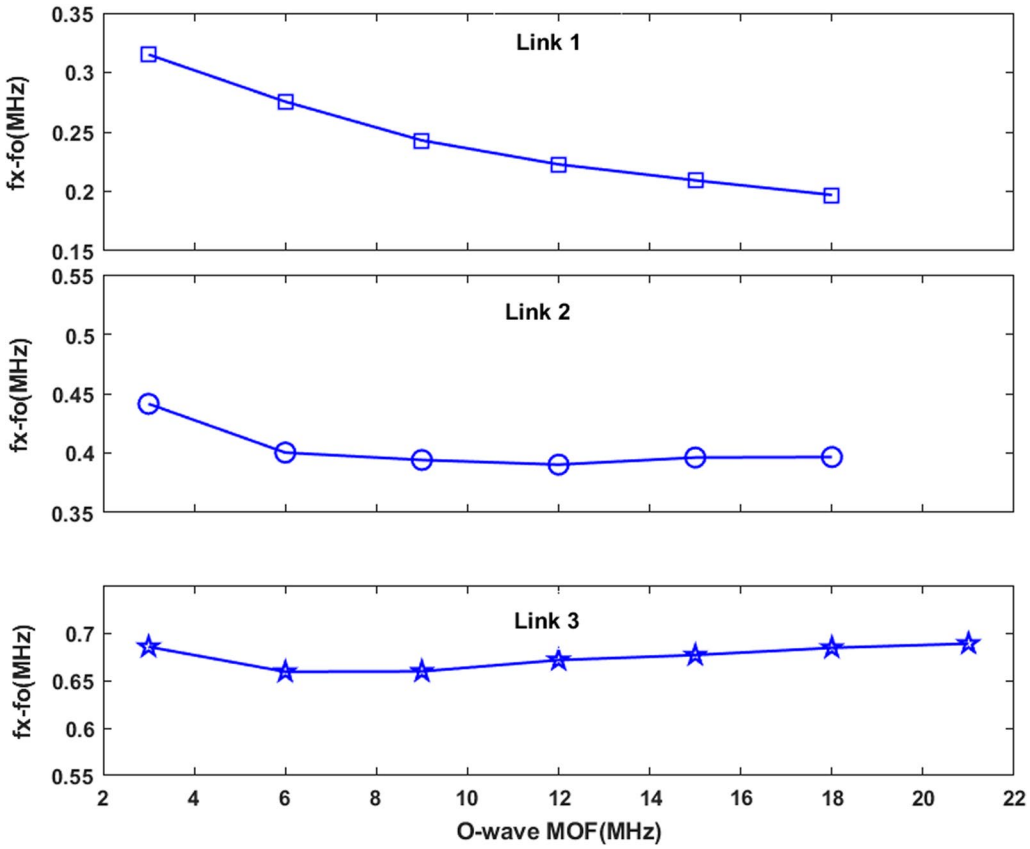

Fig. 8 Correlation between the separation and the O-wave JF

in spring and summer is about 100 km, which is evidently larger than the difference between spring's hmF2 and summer's hmF2. Further analysis of the summer oblique ionograms shows that the F2-layer trace uplifts mainly occur when a completely developed F1-layer or strong Es-layer exists. One possible interpretation is that the existence of the completely developed F1-layer or strong Es-layer increases the transmission length of F2 mode which further increases the difference in ray-path between O- and X-wave, thereby the frequency difference between O- and X-wave increases. In order to verify this idea, a 3D magnetoionic Hamiltonian ray-tracing toolbox PHaRLAP is adopted to simulate the changes in ray path when the F1-layer exists or not, which uses Jones and Stephenson (1975) 3D ray-tracing code for ray path calculation. The ionospheric model used in this verification is 'IRI-2016' with the 'F1 model' being set to be 'Scotto-1997 no L' or 'None' to simulate the condition with F1-layer or without F1-layer. Figure 12 presents the synthesized oblique ionograms with and without the F1-layer. It can be seen that when there is a F1-layer, the trace of the F2-layer is lifted by about 30 km, the JF of F2-layer O-wave is reduced by 0.15 MHz, and the separation gets larger by 0.025 MHz compared with the condition without F1-layer. Then, we set the critical frequency of the F1-layer to increase by 1.5 MHz, run the ray-tracing program, and find that the separation $f_X - f_O$ becomes larger by 0.05 MHz, which is close to the average value (0.062 MHz) of the difference in the separation between summer and other seasons during daytime. In summary, we believe that the separation is mainly affected by hmF2 above the reflection point, and the separation increases when there is an F1-layer or strong Es-layer.

Another noteworthy phenomenon is that the separation on east–west path is slightly weakened under active geomagnetic conditions compared to quiet conditions. Based on Davis's approximation formula for the cases of magnetic east–west propagation, it is known that the separation is proportional to the square of f_H, where $f_H = \frac{eF}{2\pi m}$ (F is the total intensity of the Earth's geomagnetic field; e and m are the charge and mass of electron, respectively). In general, F at any point on the Earth's surface is more than 30,000 nT (Davies 1990). During the main phase of the magnetic storm, F may drop by 40–500 nT (Clilverd et al. 1998). It may cause

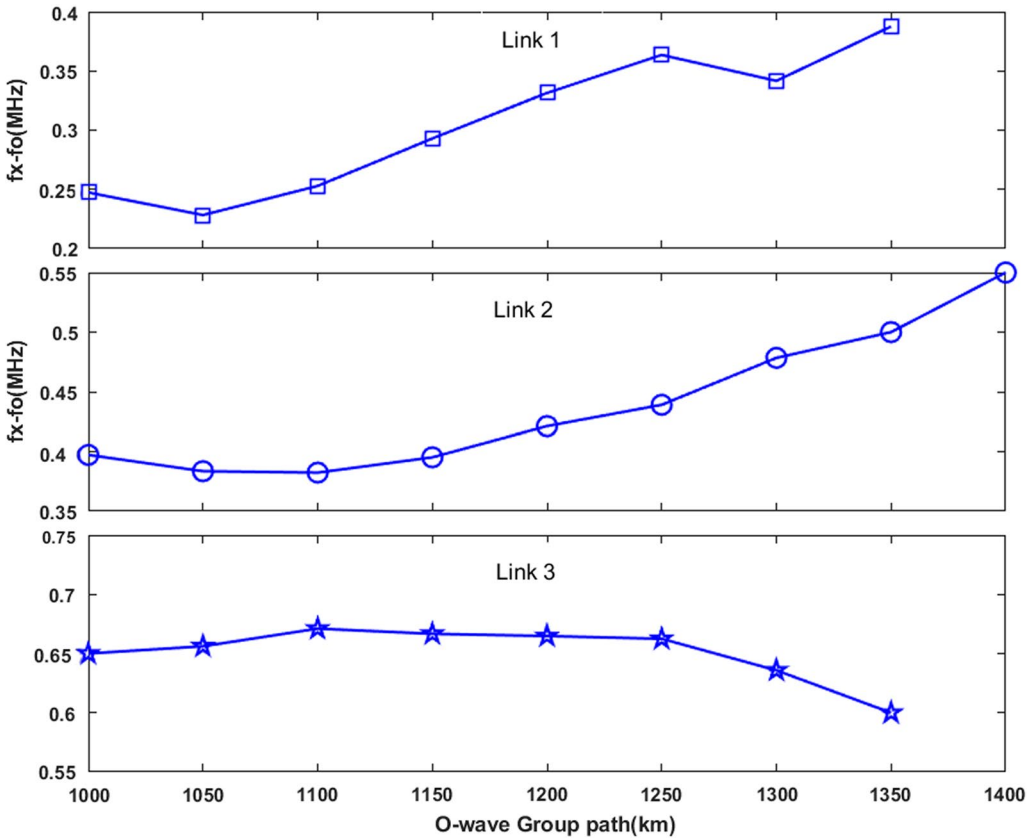

Fig. 9 Correlation between the separation and O-wave group path

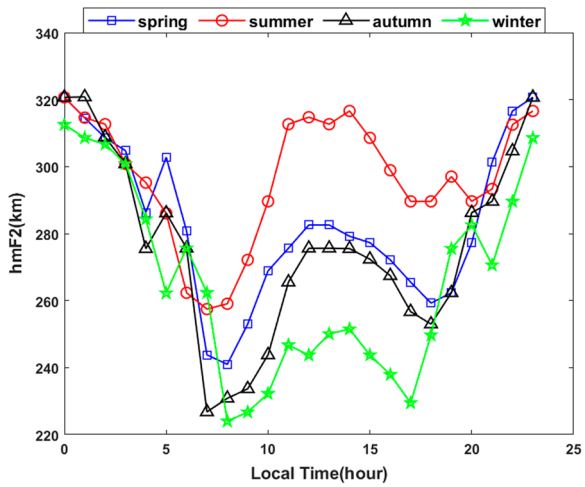

Fig. 10 Seasonal variation of the peak height of the F2-layer observed in Xi'an; blue, red, black, and green lines represent spring, summer, autumn, and winter, respectively

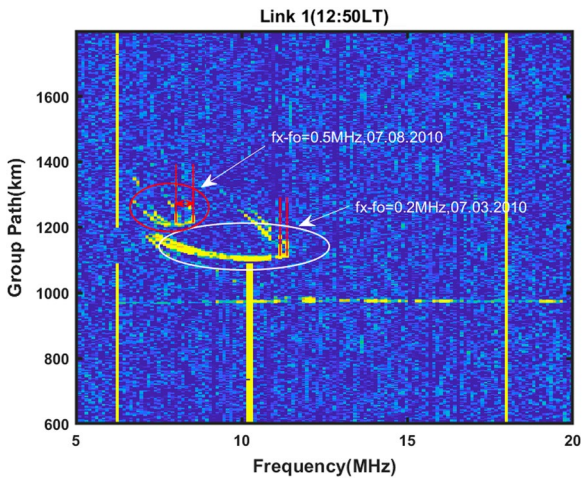

Fig. 11 A typical set of oblique-incidence F2-layer traces at 12:50 LT in summer and spring, the F2-layer trace circled by a red ellipse was taken on August 7, 2010, and the trace circled by a white ellipse was taken on March 7, 2010

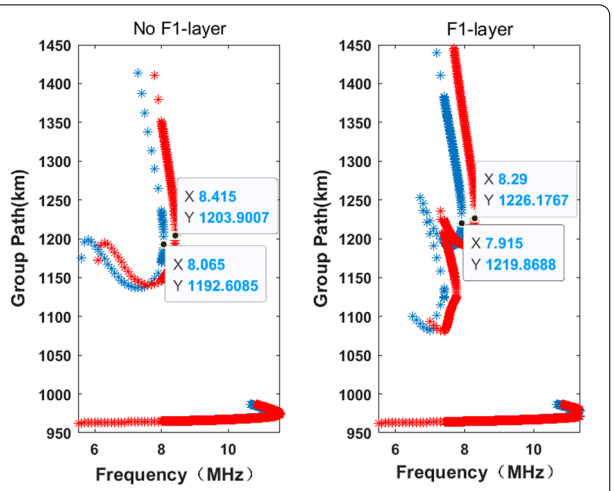

Fig. 12 Synthesized oblique ionograms with and without F1-layer

a 0.3–3% drop in the separation, which is consistent with the statistical one (about 0.01 MHz). However, we must keep in mind that the reduction of the separation during geomagnetic disturbance is lower than the frequency resolution. So we argue that the separation is less sensitive to magnetic disturbances.

Case of quasi north–south propagation

Our statistics confirms that the separation on the quasi north–south propagation path is the most significant among the three links, which agrees with previous studies. This means that the magneto-ionic splitting on north–south path is more prominent than that on east–west path. Furthermore, the separation on north–south path does not vary significantly with the local time and season, and also has a weak correlation with O-wave JF and group path. In addition, the comparison between Figs. 5 and 10 shows that the diurnal variation trend of the separation on Link 3 is obviously different from that of hmF2. In the book "Ionospheric radio", Davies (1990) has pointed out that the angle between the wave normal and the magnetic field is small in the case of north–south or south–north propagation, so the propagation is quasi-longitudinal, and the separation in JFs between O- and X-wave is approximately expressed as $f_X - f_O \approx f_H cosI$. It shows that the separation is mainly determined by the gyrofrequency f_H and the magnetic dip I, and is hardly affected by the ionospheric activity. This may be the reason why the separation on Link 3 has a weak correlation with local time, season, O-wave JF and group, and hmF2. According to the analysis in the previous section, the change of the total intensity F is very small compared to the background field, which cannot cause significant changes in f_H and I. So there is no obvious abnormality in the mean value of the separations during the period of geomagnetic disturbance.

Simulation of the dependence on solar activity variations

The aforementioned analysis shows that the separation to east–west path is susceptible on ionospheric variability, and it cannot be interpreted well by Davies's relationship. Davies (1990) pointed out that the left-handed O-wave and the right-handed X-wave introduced by magneto-ionic splitting traveled different paths in the ionosphere and it was not possible to integrate analytically to obtain the precise ray path, but it was practical to do so by means of point-to-point ray tracing. Therefore, we make use of 3D ray tracing to analyze the dependence of the separation on solar activity.

The diurnal variations of the separation are conducted on Link 1 covering three levels of solar activity (R = 10, 70, and 120, respectively, represent the low, medium, and high solar activity) and four months (January, April, July, and October, characterize four different seasons), as shown in Fig. 13.

It is observed that the double-peak variation of the separations with one maximum in local noon and another maximum in local midnight or pre-sunrise is favored for all solar activities in different seasons. In January and October, the separation at night is more prominent than that during the daytime, and the maximum at night occurs at low solar activity while the largest value during daytime is found at the high solar activity. In April, the separation during the low solar activity phase is higher at night and slightly lower in the daytime which is consistent with the observations over Link 1, while the separations during medium and high solar activities are larger in the daytime than that at night. In July, the separation during the day is more obvious when compared with that at night for all solar activities. According to IRI, the F1-layer critical frequency at the midpoint of link 1 is calculated, and the result shows the occurrence of the F1-layer is higher than that in January, April, and October. Combining the previous simulation, we infer that the increase in the occurrence of F1-layer in IRI model is the main factor responsible for the obviousness of the separation during the day in July.

Simulation of the dependence on length and direction of propagation

In order to investigate sensitivity to the length and direction of propagation, calculations were performed for different path configurations with a central receiver at Xi'an. The results obtained by the 3D ray-tracing method discussed in this paper are shown in Fig. 14. The figure above shows the variability of the separation as a function of the direction of propagation for two different transmission lengths that are 1000 km and 2000 km, while the figure below shows the variability of the separation against the length of propagation for four different

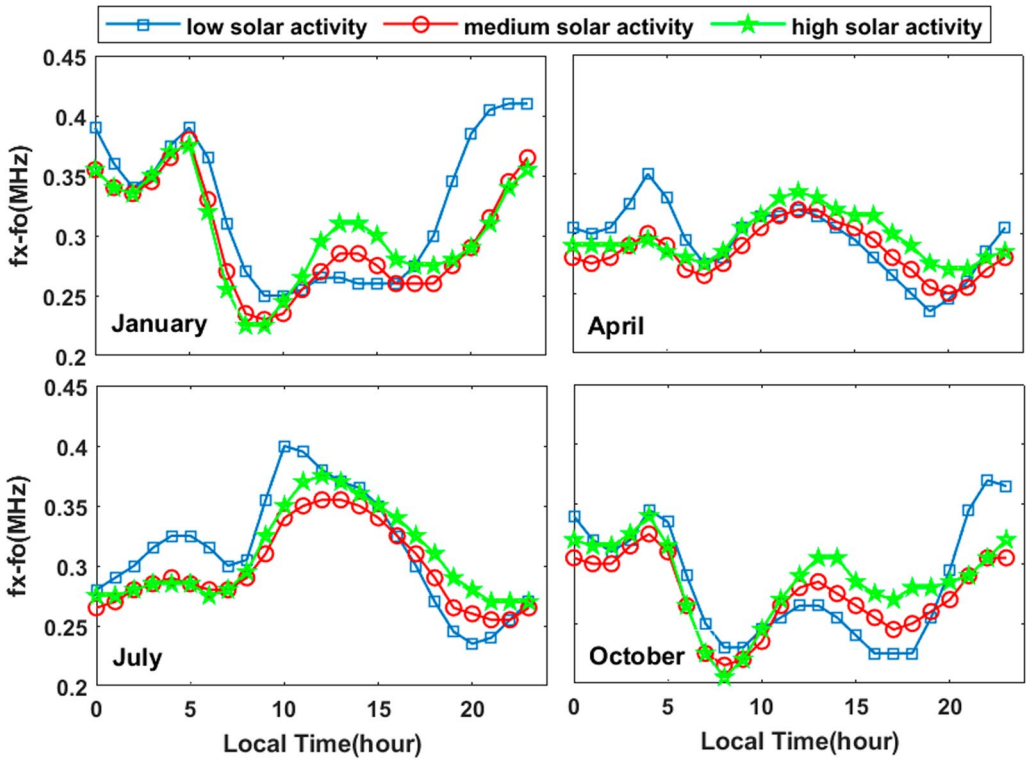

Fig. 13 Solar activity variability of the separation simulated using 3D ray-tracing method; blue line for low solar activity, red line for medium solar activity, and green line for high solar activity

transmission azimuth angles of 45°, 90°, 145°, and 180°. As we can see, the separation varies approximately as the cosine function of the propagation direction with maximums at north–south direction and minimums at east–west direction in mid-latitude China region. Due to the different transmission directions, the separations on radio links with ground range greater than 500 km present obviously distinct patterns. For east–west propagation path, the separation decreases to a minimum near ground range of 2000 km and then increases very slowly with increasing ground range, while for north–south propagation path, it gradually increases with increasing ground range. The relationship of the separation with transmission length is partly inconsistent with the results simulated by Bennett et al. (1994) which show a tendency to decrease below 1000 km and then increase very slowly for a case with azimuth equal to 0 (of north–south propagation). Based on the use of an equivalent operating frequency, Bennett took into account the effect of the Earth's magnetic field in an analytical ray-tracing program. The use of the equivalent operating frequency led to deviations in the ray path, which caused calculation errors, and resulted in the inconsistency with 3D ray tracing.

Summary and conclusions

We have presented a statistical and simulation study on the separation in JFs between O- and X-wave based on oblique sounding data recorded by three mid-latitude paths within China and 3D ray-tracing program. The dependence of the separation on local time, season, geomagnetic activity, O-wave JF, and group path is statistically analyzed based on observed oblique ionograms over three mid-latitude paths within China, and the influences of the length of the propagation circuit, the direction of propagation and the solar activity variability have been analyzed by a ray-tracing program. The major conclusions are summarized as follows:

(1) The separation on east–west path is susceptible to ionospheric variability, which is inconsistent with previous analysis that the separation does not depend strongly on the ionospheric plasma distribution (Bennett et al. 1994), while the separation on north–south path does not show significant correlation with local time and season variations.
(2) The separation on the east–west path depends on the local time, season, and solar activity. There is a general diurnal variation, which mainly relates to the diurnal variation of hmF2 above the reflection

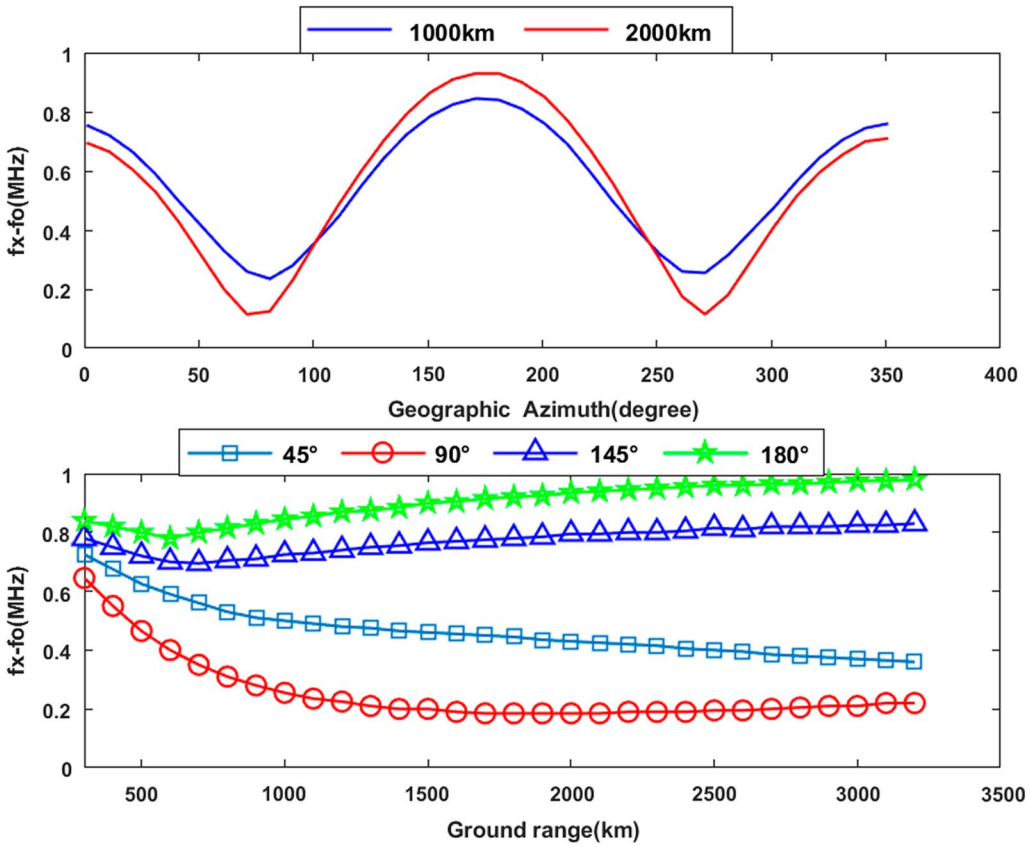

Fig. 14 Relationship of the separation with length and direction of propagation; upper diagram shows variability on direction of propagation, lower diagram shows variability on length of propagation

point. The most striking feature is summer anomaly showing that the separation during daytime is more prominent than that at night in summer, while it is the opposite in other seasons. One possible interpretation is the effect of refraction in a completely developed F1-layer or strong Es-layer.

(3) The separation varies approximately as the cosine function of the propagation direction owning two maximums at north–south direction and two minimums at east–west direction in the mid-latitude China region. This feature is consistent with previous research results that the magneto-ionic splitting is less for an east–west path than a north–south path.

(4) The separations on different transmission azimuths present distinct patterns. For east–west propagation path, the separation decreases to a minimum near ground range of 2000 km and then increases very slowly with increasing ground range, while for north–south propagation path, it gradually increases.

In order to automatically extract F2-layer O- and X-wave parameters from oblique ionograms to achieve the best performance, a study for the behavior of separation in JFs between O- and X-waves is always useful and worthy. Our contribution is achieved through two aspects: regarding experimental observation, the general diurnal tendency and summer anomaly of the separation are firstly proposed; regarding simulation, provides interesting insights into the dependence of the separation on solar activity, length, and direction of propagation and gains a different conclusion from the previous analysis.

The future work will be to take more experimental data during the medium and high solar activity years to verify the accuracy of the simulation results.

Abbreviations

JF: The frequency at which the high- and low-angle rays join; O-mode or O-wave: The ordinary mode or wave; X-mode or X-wave: The extraordinary mode or wave; HF: High frequency; LOF: The lowest observed frequency; MOF: The maximum observed frequency; FMUF: The highest useable frequency of one-hop F layer; FHLOF: The lowest observed frequency of the high-angle ray along one-hop F layer; FLLOF: The lowest observed frequency of the low-angle ray along one-hop F layer; 2FMOF: The maximum observed frequency of the two-hop F layer; CRIRP: China Research Institute of Radio-wave Propagation; GPS: Global Positioning System; DSTO: Defence Science and Technology Organization.

Acknowledgements
The authors acknowledge the Data Center of the China Research Institute of Radiowave Propagation for help with ionograms collection. The authors would like to thank Dr. Shuji Sun and Dr. Boya Li for proofreading this manuscript. The authors would also like to thank the anonymous referee for the useful comments and suggestions for improving the paper.

Author contributions
SFJ designed the study, analyzed the data, and wrote the manuscript. WXR, ZHB and ZB contributed related analysis on data. BPP contributed related analysis on simulation. ZB and CHY helped with the text of the paper, particularly with the introduction and comparison with previous works. All co-authors contributed to the revision of the draft manuscript and the improvement of the discussion. All authors read and approved the final manuscript.

Authors' information
FengJuan Sun is currently a Ph.D. student at Wuhan University. She also is a Senior Engineer at the China Research Institute of Radiowave Propagation. She has authored and coauthored 6 patents and over 8 journal articles. Her current research interests are in ionospheric radiowave propagation and its influence on HF radar. Dr. XianRong Wan is currently a Professor and Ph.D. candidate supervisor at Wuhan University whose main research interests include the design of new radar system such as over-the-horizon radar, passive radar, and array signal processing. Dr. HongBo Zhang is currently a senior engineer at the China Research Institute of Radiowave Propagation. He has participated in the activities of the ITU-R study group 3 and has submitted about 3 contributions to the ITU-R SG3. Master Bao Zhou and HongYan Cao are currently senior engineers at the China Research Institute of Radiowave Propagation. Their research interests are in shortwave frequency forecasting, spectrum monitoring, and management. Dr. PanPan Ban is a Ph.D. student at Wuhan University. Her current research interests are in ionospheric forecasting and ionospheric radiowave propagation.

Funding
This work was supported by the National Natural Science Foundation of China (Grant No. 61931015), Innovation Group Project of the Natural Science Foundation of Hubei Province (Grant No. 2021 CFA002), and Stable-Support Scientific Project of China Research Institute of Radiowave Propagation (Grant No. A132011W16). The funds from Grant No. A132011W16 were used for data collection and analysis. The funds from Grant Nos. 61931015, 2021 CFA002 were used for manuscript preparation.

Availability of data and materials
The 3-hourly Kp index is available in the website: http://wdc.hugi.kyoto-u.ac.jp/. Regretfully, the oblique ionograms data used in this manuscript cannot be shared because they belonged to the China Research Institute of Radio-wave Propagation (CRIRP).

Declarations

Ethics approval and consent to participate
Not applicable.

Consent for publication
Written informed consent was obtained from study participants for participation in the study and for the publication of this report and any accompanying images. Consent and approval for publication was also obtained from Wuhan University and China Research Institute of Radio-wave Propagation.

Competing interests
The author declares no competing interests.

Author details
[1]Radio Detection Research Center, School of Electronic and Information, Wuhan University, Wuhan 430072, China. [2]China Research Institute of Radio-Wave Propagation, 36 Xianshan Road, Chengyang District, QingDao 266107, China. [3]Xidian University, Xian 710068, China.

Received: 2 February 2022 Accepted: 15 December 2022
Published online: 27 December 2022

References

Agy V, Davies K (1959) Ionospheric investigations using the sweep-frequency pulse technique at oblique incidence. J Res Nat Bureau Stan D Rad Prop 63(2):151–155
Bennett JA, Chen J, Dyson PL (1994) Analytic calculation of the ordinary (O) and extraordinary (X) mode nose frequencies on oblique ionograms. J Atmos Terr Phys 56(5):631–636
Bradley PA, Eccles D, King JW (1970) Ionospheric probing using pulsed radio waves at oblique incidence. J Atmos Terr Phys 32:499–516
Cervera MA, Harris TJ (2014) Modeling ionospheric disturbance features in quasi-vertically incident ionograms using 3Dmagnetoionic ray tracing and atmospheric gravity waves. J Geophys Res Space Phys 119:431–440
Chemogor LF, Garmash KP, Guo Q, Luo Y, Rozumenko VT, Zheng Y (2020) Ionospheric storm effects over the People's Republic of China on 14 May 2019: results from multipath muti-frequency oblique radio sounding. Adv Space Res 66(2):226–242. https://doi.org/10.1016/j.asr.2020.03.037
Clilverd MA, Clark TDG, Clarke E, Rishbeth H (1998) Increased magnetic storm activity from 1868 to 1995. J Atmos Solar Terr Phys 60:1047–1056
Davies K (1990) Ionospheric radio. London, United Kingdom: The Institution of Engineering and Technology.
Dyson PL, Bennett JA (1979) General formulae for absorption of radio waves in the ionosphere. J Atmos Terr Phys 41:367–377
Dyson PL, Bennett JA (1980) A universal chart for use in relating ionospheric absorption to phase path and group path. IEEE Trans Antennas Propag 28(3):380–384
Harris TJ, Cervera MA, Pederick LH, Quinn AD (2017) Separation of O/X polarization modes on oblique ionospheric soundings. Rad Sci 52(12):1522–1522. https://doi.org/10.1002/2017RS006280
Heitmann AJ, Gardiner-Garden RS (2018) A robust feature extraction and parameterized fitting algorithm for bottom-side oblique and vertical incidence ionograms. Radio Sci 54(1):115–134. https://doi.org/10.1029/2018RS006682
Ippolito A, Scotto C, Sabbagh D, Sgrigna V, Pdi M (2015a) A procedure for the reliability improvement of the oblique ionograms automatic scaling algorithm. Radio Sci 51:454–460. https://doi.org/10.1002/2015RS005919
Ippolito A, Scotto C, Francis M, Settimi A, Cesaroni C (2015b) Automatic interpretation of oblique ionograms. Adv Space Res 55:1624–1629
Jones RM, Stephenson JJ (1975) A versatile three-dimensional ray tracing computer program for radio waves in the ionosphere. Washington DC, USA:U.S. Dept. Commerce, Office Telecommun
Kopka H, Moller HGM (1968) MUF calculations including the effect of the Earth's magnetic field. Radio Sci 1(3):53–56
Liu Z, Fang H, Weng H, Wang S, Niu J, Meng X (2019) A comparison of ionosonde measured foF2 and IRI-2016 predictions over China. Adv Space Res 63(6):1926–1936
Lundborg B, Broms M, Derblom H (1995) Oblique sounding of an auroral ionospheric HF channel. J Atmos Terr Phys 1:51–63
Pezzopane M, Pietrella M (2008) Interobl: an interactive software tool for displaying and scaling oblique ionograms. Comput Geosci 34:1577–1583
Phanivong B, Chen J, Dyson PL, Bennet JA (1995) Inversion of oblique ionograms including the Earth's magnetic field. J Atmos Terr Phys 57:1715–1721
Rao NN (1973) A note on the analysis of oblique ionograms. J Atmos Terr Phys 35:1561–1563
Reily MH, Kolesar JD (1989) A method for real height analysis of oblique ionograms. Radio Sci 24:575–583. https://doi.org/10.1029/RS024i004p00575
Rogov DD, Vystavnoi VM, Blagoveshchenskaya NF, Baryshev PE, Kalishin ASK (2021) Russian high-latitude network of oblique ionospheric sounding. Russ Meteorol Hydrol 46(4):217–224
Storey LRO (1960) The joint use of the ordinary and extraordinary virtual height curves in determining ionospheric layer profiles. J Res Nat Bur Stan D Radio Prop 64(2):111–124
Wang N, Guo LX, Zhao ZW, Ding ZH, Lin LK (2018) Spread-F occurrences and relationships with foF2 and h'F at low-and mid-latitudes in China. Earth Planets Space. https://doi.org/10.1186/s40623-018-0821-9

Publisher's Note